https://doi.org/10.48048/tis.2024.7168

Enhanced Osteogenic Differentiation of Human Mesenchymal Stem Cells with Synthetic Coral Matrix in the Presence or Absence of Growth Factors from the Platelet Rich-rich Plasma

Erlina Sih Mahanani[1], Ika Dewi Ana[2,3,*], Indra Bachtiar[4] and Yin Xiao[5]

[1]Department of Dental Biomedical Sciences, Faculty of Dentistry, Universitas Muhammadiyah Yogyakarta, Bantul 55183, Indonesia
[2]Department of Dental Biomedical Sciences, Faculty of Dentistry, Universitas Gadjah Mada, Yogyakarta 55281, Indonesia
[3]Research Collaboration Centre for Biomedical Scaffolds, National Research and Innovation Agency, Universitas Gadjah Mada, Yogyakarta 55281, Indonesia
[4]Stem Cells and Cancer Institute, Jakarta 13210, Indonesia
[5]School of Medicine and Dentistry, Griffith University, Gold Coast Campus, Queensland 4222, Australia

([*]Corresponding author's e-mail: ikadewiana@ugm.ac.id)

Received: 4 June 2023, Revised: 19 July 2023, Accepted: 23 July 2023, Published: 20 December 2023

Abstract

To solve problems in using natural sea corals with high biocompatibility, good osteoconductivity, and ideal degradability, a synthetic three-dimensional coral matrix was fabricated and observed for its capability to enhance osteogenic differentiation of human mesenchymal stem cells (h-MSCs), in the presence or absence of growth factors (GFs) supplied from platelet-rich plasma (PRP). Expressions of runx, osterix, and osteocalcin were investigated, following cell attachment, and proliferation analysis. Ectopic bone formation in nonosseous tissues of Sprague-Dawley rats at predetermined time intervals was investigated, including mineralized tissue growth *in vivo*. The 3D synthetic coral matrix (SCM) can interact with the GF cocktail in the PRP and MSCs to generate and secret bone extracellular matrix (ECM) both *in vitro* and i*n vivo*. The matrix supplied with GF cocktail from the PRP provided an ideal microenvironment for MSCs to attach, proliferate, and differentiate into osteoblast faster, as indicated by the expression levels of runx2, osterix, and osteocalcin. The high capability of SCMs to enhance bone formation has been proven by the formation of ectopic bones in the nonosseous environment. The incorporated PRP provided blood proteins such as fibrin to slow down matrix degradation, whereas GF supplied by the PRP stimulated h-MSCs to attach and proliferate onto the matrix. Moreover, the GF supplied by the PRP enhanced osteogenic differentiation and mineralization, accelerating bone regeneration. Valorization phases are needed to apply the SCM for bone tissue engineering in clinics.

Keywords: Synthetic coral matrix (SCM), Scaffold, Growth factors, Platelet rich plasma (PRP), Human mesenchymal stem cells (h-MSCs), Bone tissue engineering

Introduction

From the perspective of biomedical sciences and tissue engineering, providing a microenvironment mimicking the physiological and physicochemical conditions of the extracellular matrix (ECM) of the native tissue has become a research focus to allow tissues to regenerate well in damaged or injured areas. The biomimetic microenvironment will accommodate diverse host processes toward wound healing, i.e., angiogenesis, vasculogenesis, cell migration, cell proliferation, cell orientation, inflammation, and immune responsiveness, because it can be a reservoir for signaling factors. The biomimetic microenvironment such as the native ECM also facilitates attachment sites for cell surface receptors.

In the context of tissue engineering, this biomimetic microenvironment, which acts as synthetic ECM, is called a scaffold. Scaffolds optimize cellular interactions within the body, which results in the successful integration of the scaffold and biophysical and biochemical cues into the host tissue [1,2], leading to cell differentiation and ECM generation to form new tissues [3]. Although the newest technological advancement in tissue engineering has reached the concept of intracellular reprogramming [4], synthetic ECM is still the focus of tissue engineering science.

In bone tissue engineering, congenital, age-related, or acquired bone damage or injury could result in bone loss [5-8]. As reported previously, more than a million people are treated for skeletal problems

annually in the fields of orthopedic surgery, plastic surgery, maxillofacial surgery, and neurosurgery [9]. Although bone tissues have an excellent capacity to regenerate and spontaneously repair damage [10,11], their self-repair capability must be enhanced in the presence of a large critical defect. In this condition, a well-affirmed method to accelerate bone regeneration is a system consisting of scaffolds as synthetic ECM, signaling molecules, and cells, either alone or in combination [12].

In bone tissue engineering, scaffolds will support and induce cells to proliferate and differentiate properly [13] and form three-dimensional (3D) tissue structures as a substitute for damaged tissues [14]. For this, a wide range of hybrid biomaterials with tunable biophysical and biochemical characteristics have been developed as scaffolds in bone tissue engineering [15]. Among them is the coral scaffold, which is biocompatible, osteoconductive, and resorbable and can provide a delivery system for bone growth factors [16]. Sea corals have pores like human spongy bones and contain $CaCO_3$ in the form of calcite. Coral scaffolds have been utilized several decades ago as a bone substitute material, without any further mineralogical changes [17]. When accompanied by growth factor recombinant bone morphogenic protein 2 and mesenchymal stem cells (MSCs), the use of coral scaffolds resulted in the repair of cranial defects [16].

Moreover, in some cases, the use of coral scaffolds requires other components, i.e., cells, and signaling molecules to regenerate damaged tissues [16-18], particularly in areas with extensive and large damage (critical defects). Stem cells (SCs) from the bone marrow and umbilical cord tested with coral scaffolds could grow and differentiate into osteoblasts [18]. However, the exact mechanism of how other components such as GFs and cells can result in accelerated bone regeneration is still unclear. The underlying processes for the bones to regenerate in the presence of coral scaffolds with or without accompanying GFs and MSCs remain questionable [19,20]. In addition, the excessive use of original sea corals may damage the natural habitats of the corals.

To address the issues of the unclear yet regenerative mechanism in the use of coral scaffolds for bone tissue engineering and the limitation on the use of natural corals, in this study, we continued our previous studies on mimicking coral structures [19]. The capability of the formulated SCM from endotoxin-controlled bovine gelatin and $CaCO_3$ in inducing MSC differentiation into osteoblasts in relation to bone tissue regeneration processes was investigated *in vitro* and *in vivo*, with and without the presence of a growth factor cocktail derived from platelet-rich plasma (PRP). An *in vivo* study was conducted by implanting SCMs with and without PRP and MSCs in a nonosseous environment.

Materials and methods

Study design and ethical approval

In this experimental laboratory study with a post-test control group, ethical clearance for the *in vitro* and *in vivo* study protocols was applied. This study was approved by the research ethics committee (No. 694/KKEP/FKG-UGM/EC/2014), which has been renewed annually and amended for improvement when needed until the end of the study. Informed consent was obtained from eligible voluntary donors for PRP preparation.

SCM preparation

To provide SCMs with the intended properties, gelatin and calcium carbonate in a 5:5 ratio inside 10 % w/v were prepared from $CaCO_3$ (Wako Co., Tokyo, Japan) and bovine gelatin (Nitta, Osaka, Japan). The fabrication procedure for the development of SCMs was based on a previous study [19]. The obtained SCMs were checked for their macro- and microstructural appearance, physical, and chemical properties, microstructure, and Zeta-potential by scanning electron microscopy (with platinum coating) using an SU-35000 microscope (Hitachi, Tokyo, Japan) and a particle size analyzer (Horiba SZ-100, Horiba, Japan). The swelling ratio, degradation profile, PRP-loading capacity, and PRP-release profile from the matrix were measured. The swelling ratio and degradation profile were evaluated using a UV-vis spectrophotometer (UV-1800, Shimadzu, Japan), referring to procedures published previously [21]. The PRP preparation and analysis of PRP-loading capacity and release profile were also conducted based on a previous study [21-24]. Before all *in vitro* cell and animal studies, the obtained SCMs were sterilized with ethylene oxide gas under dry conditions at 40 °C.

Preparation of PRP

Inclusion criteria were as follows: Voluntary healthy donors who had no systemic diseases, hepatitis, or HIV infections during PRP preparation. Human PRP was obtained from the eligible voluntary donors who filled out and signed informed consent. Then, 10 mL of whole blood was collected from each donor

and placed in a citrate Vacutainer (BD, NY, USA) for platelet counting [19,24]. The whole blood was then centrifuged for 10 min at 4 °C and 1700 rcf, and platelets were collected into another new tube. The collected platelets were transferred into microtubes (Axygen, CA, USA), centrifuged again for another 10 min at 4 °C and 3100 rcf in a refrigerated centrifuge (Eppendorf 5417 R, Hamburg, Germany), and PRP was ready for the study.

Preparation and characterization of MSCs

Human MSCs (h-MSCs) were isolated from Wharton's jelly in the human umbilical cord after delivery using the explant method, and they were handled following the established national standard protocol for isolation, culture, and use of MSCs derived from the umbilical cord at the accredited laboratory of Stem Cells and Cancer Institute of PT Kalbe Farma Tbk. After isolation, MSCs were cultured in a minimum essential medium growth media supplemented with Glutamax (Gibco, Waltham, MA, USA), with fetal bovine serum (Sigma-Aldrich, St. Louis, MO, USA), fungizone, and penicillin–streptomycin (Gibco). Passage six of the h-MSCs was then characterized by fluorescence-activated cell sorting (Becton Dickinson, Franklin Lake, NJ, USA) with surface markers (**Figure 1**).

Cell studies

The group assignment for cell studies is presented in **Table 1**. For h-MSC attachment and proliferation studies, SCMs with, or without PRP were tested. The cell attachment and proliferation studies for each group were conducted following methods published in a previous study [19]. By using the dye exclusion method, the percentage of the attached cells at 3, 6, and 24 h and the number of proliferated cells 24, 48, and 72 h after incubation were determined.

Table 1 Test group assignment to observe the attachment, proliferation, differentiation, and ectopic bone formation capability of MSCs on the synthetic coral matrix (S) with (P1) and without GFs from PRP (P0).

Type of test	Treatment group	Control croup	Notes
Cell attachment	S1P0M1-SM S1P1M1-SM	S0P0M1-SM	The control group was designed to check the capability of MSCs to attach in the well without SCM and PRP.
Cell proliferation	S1P0M1-SM S1P1M1-SM	S0P0M1-SM	The control group was designed to check the capability of MSCs to proliferate in the well without SCM and PRP.
Cell differentiation (Runx2, Osterix, and Osteocalcin Expressions)	S1P0M1-OM S1P1M1-OM	S0P0M1-OM S1P1M1-SM	In S0P0M1-OM, the control group was designed to assess the capability of MSCs to differentiate on the well in an osteogenic medium, without SCM, and PRP. In S1P1M1-SM, it was designed as a positive control in a standard medium (non-osseous environment), wherein the SCM was incorporated with PRP for MSCs to differentiate.
Ectopic bone formation	S1P0M1 S1P1M1	S1P0M0 S1P1M0	The control group consisted of SCM only, without growth factors and cells, and SCM incorporated with growth factors from the PRP without cells.

*Remarks: S = SCM, P = PRP, M = MSC, 0 = without, 1 = with, OM = osteogenic medium, SM = standard medium.

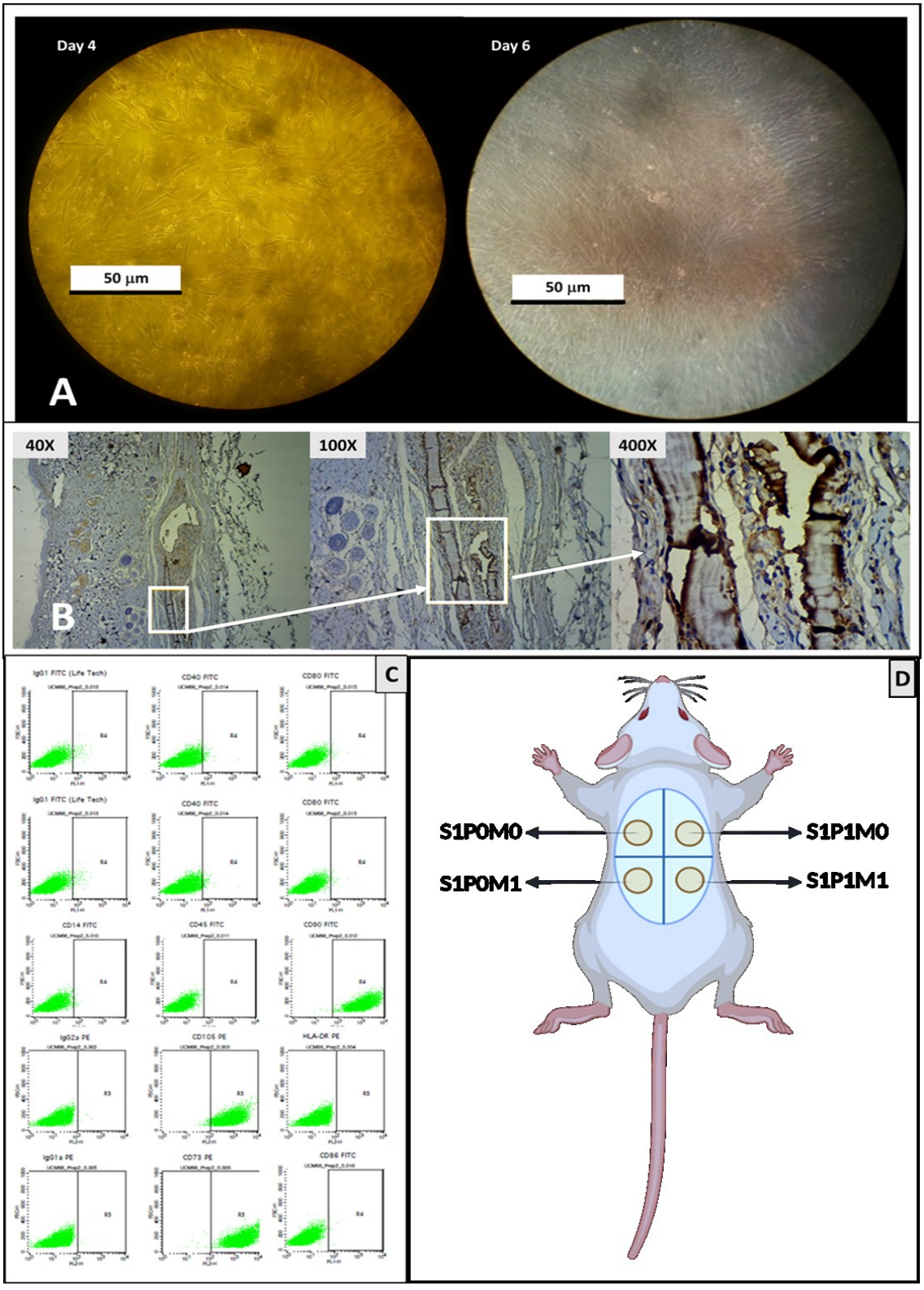

Figure 1 Methods used in the study. For the study, h-MSCs were isolated from Wharton's jelly in the human umbilical cord after delivery using the explant method. A) After 4 and 6 days of incubation, 60% confluency was reached. B) Histological observation after immunohistochemistry (IHC) staining was conducted at 400× magnification. C) Identification on h-MSCs resulted in negative surface marker toward CD45, CD19, CD86, CD80, CD14, CD34, HLADR, and positive toward CD73, CD90, and CD105. D) Assignment for subcutaneous implantation on rat dorsum.

Cell attachment onto the SCM was also observed by SEM. After incubation for 48 h, the culture was washed with phosphate-buffered saline (PBS) solution three times and fixed with 2.5 % glutaraldehyde. A dehydration series was conducted at 50, 70 and 90 % before final dehydration with 100% alcohol concentration, two times for 30 min each. Specimens were then dried at room temperature, platinum coated, and observed under a JEOL-JSM 6510 microscope (JEOL Ltd., Tokyo, Japan).

For h-MSC differentiation, in all assigned groups, cells were incubated in 6-well plates for 3 days in a standard growth medium to achieve an average of 60 % attached cell confluency. The medium was then replaced with either a standard medium (SM) or an osteogenic medium (OM) based on the group assignment with 1.2×105 cells/well, incubated for 7, 14, and 21 days, with medium replacement every 3 - 4 days, and used for cell differentiation analysis. Upon reaching the predetermined incubation duration, h-MSCs were harvested by detaching the cells from the synthetic matrix and/or well plate using trypsin EDTA (Gibco). Then, the cells were washed with sterilized PBS three times, centrifuged, and subjected to RNA isolation with RNeasy Minikit (Qiagen, Germantown, MD, USA). The isolated RNA was then used to prepare cDNA using the iScript cDNA Synthesis Kit (BioRad, Hercules, CA, USA).

Then, the CDNA was used for osteogenic marker observation on day 7 for runx2, day 14 for osterix, and day 21 for osteocalcin with GDPH as the housekeeping gene. The expression of osteogenic markers was analyzed by reverse-transcriptase polymerase chain reaction (RT-PCR) using Veriti 96-well thermal cycler (Applied Biosystem, Waltham, MA, USA) and gel doc electrophoresis using i-Mupid J (Eurogentec, Seraing, Liege, Belgium) at 302-nm UV wavelength. Then, the results of the RT-PCR and electrophoresis were visualized by ImageJ, by referring to Gene Bank ID AF001450, AF477981, and NM_199173.4 for runx2, osterix, and osteocalcin, respectively.

Animal model and subcutaneous implantation

The animal protocol for this study was approved by the Research Ethics Committee of The Faculty of Dentistry, Universitas Gadjah Mada (UGM). In this study, 24 male Sprague-Dawley rats (3 months old; weight, 250 - 300 g) were used. This study followed the national guidelines for the care and use of laboratory animals. The animals were housed in cages located at the Integrated Research and Testing Laboratory, Gadjah Mada University (UGM). Surgery was performed aseptically under general anesthesia by intramuscular (i.m.) injection of ketamine (11 - 22 mg/kg body weight) in combination with xylasin (0.55 - 1.1 mg/kg body weight). To reduce the risk of perioperative infection, the rats were treated with antibiotics, that is, Interflox-100 (Interchemix, Holland) at 10 mL/20 - 40 kg i.m. during and 3 - 5 days after surgery.

A 1-cm long dorsal pocket was created gently under the dermis. Four treatment groups were created with (0) or without (1) SCM (S), PRP (P), and h-MSCs (M), as previously described in this study. S1P0M0, S1P1M0, S1P0M1, and S1P1M1 were implanted subcutaneously on rat backs to observe ectopic bone formation (**Figure 1**). Before implantation, SCMs were prepared with punch biopsy to obtain a matrix sheet with a diameter of 6 mm and then sterilized. In the group with a growth factor cocktail from the PRP, the SCM was incorporated with 50 mL of PRP. h-MSCs were seeded on the matrix (with or without PRP) in 96-well plates with as much as 2×10^5 cells/well and incubated for a minimum of 3 h. After the insertion, the wounds were closed with vicryl 2.0 suture material. The durations for the implantation were 7 (n = 5), 14 (n = 5), 21 (n = 5), and 28 (n = 5) days. Four additional animals without any implantation were added as a negative control.

Histological procedure and analysis

After the implantation time points, the rats were euthanized using an overdose of ketamine. Immediately afterward, the dorsal part of the rats was harvested, and excess tissues were removed. The tissue was cut and fixed in 4 % paraformaldehyde and 0.1 M phosphate buffer. Dehydration in a graded series of ethanol from 50 to 100 % was conducted, and the tissue was embedded in paraffin. A series of immunohistochemistry (IHC) staining procedures with osteocalcin derived from human monoclonal antibodies (BioCare Medical, Pacheco, CA, USA) was conducted. Histological slides were evaluated by two independent observers using the calculated Kappa value to measure the mean percentage of cell positive reaction and staining intensity under a light microscope (Olympus CX21, Tokyo, Japan). The immunoreactive score (IRS) was calculated based on the method reported by Fedchenko and Reifenrath [25].

Statistical analysis

Data were expressed in mean ± standard deviation for the swelling ratio, degradation, cell attachment, and proliferation. Statistical analysis was performed with Kruskal-Wallis' analysis of variance

and the Mann-Whitney test to assess significant differences among and between groups, respectively, at a *p*-value of < 0.05. Chi-square analysis was conducted to measure the IRS, with the *p*-value also set at < 0.05.

Results and discussion

Physical and chemical properties

In this study, citrate-based dispersants were used to mobilize $CaCO_3$ into the suspension. Sodium citrate tribasic is a native dispersant in the human body. In this study, $CaCO_3$ has been equally dispersed throughout the suspension, as previously described in different studies [26,27]. As shown in **Figure 2**, the obtained matrix demonstrated 3D interconnective porosity, without calcium particles from $CaCO_3$, and with high (> 90 %) PRP-loading capacity (92.078 ± 5.70 %). The platelet diameter, which is approximately 2.5 mm [28,29], appeared to enter the 3D interconnective pore of the SCM easily.

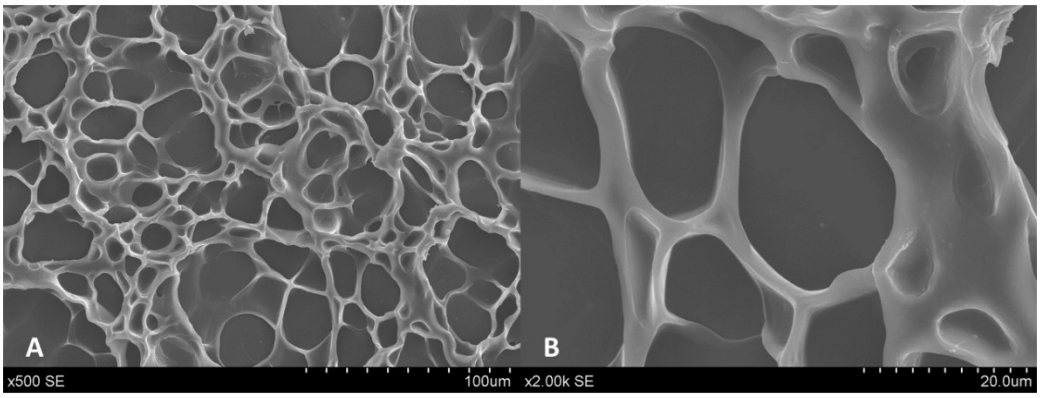

Property	Value
PRP Loading Capacity	92.078 ± 5.70 %
Zeta Potential	-0.267 ± 0.01

Figure 2 Microstructure of the SCM in A) 500× magnification and B) 2000× magnification showed a 3D interconnective pore without any microscale calcium occurrence, which indicated that calcium was dispersed equally throughout the polymer matrix. The pore size was larger than the platelet diameter of 2.5 mm. Thus, the porosity facilitated > 90 % of platelets loading into the matrix.

Upon direct contact with the body fluid, the SCM became swollen, or absorbed liquid as shown in **Figure 3**, ranging from 3.72 ± 0.45 to 4.65 ± 1.01 after 1 - 48 h of incubation. Interestingly, the degradation rate was only approximately 30 % (32.280 ± 1.01), and approximately 85.536 ± 1.71 % of the PRP were released after 96 h of incubation. It means that an adequate crosslinking procedure has been achieved to avoid direct matrix degradation, maintain the balance of water sorption in the matrix, and provide controllable release capacity [30,31].

Bone regeneration enhancement

In tissue engineering, scaffolds will support and induce cells to proliferate and differentiate properly [13] in forming 3D tissue structures as a substitute for damaged tissues [14]. In this study, the groups with SCM (S1P0M1 and S1P1M1) showed a significantly higher percentage of cell attachment ($p < 0.036$) and number of proliferated cells ($p < 0.046$) than the group without SCM (S0P0M1) 1, 3, and 24 h after incubation for attachment and 24 and 72 h after incubation for proliferation, except for 6 h ($p < 0.741$) for cell attachment and 48 h ($p < 0.138$) for cell proliferation (**Figure 4**). Besides providing larger cell-to-matrix interactions geometrically, it was assumed that Ca^{2+} and CO_3^{2-}, which are present in the SCM, support cell attachment, as previously identified [32,33].

The highest attachment and proliferation were observed after 6 and 48 h, respectively. The higher cell attachment and proliferation in S1P1M1 may be due to the appearance of transforming growth factor β (TGF-β), epidermal growth factor, and platelet-derived growth factor on the surface of the SCM [34], which

could stimulate integrin as a molecule responsible for cell attachment. Blood proteins such as fibrin, fibronectin, and vitronectin in the PRP also contributed to cell attachment [35]. The combination of SCM with fibrin from the PRP enables the slow release of growth factors and strengthens the fibrin structure as a scaffold [36,37]. The fibrin content of the PRP provided stronger matrix networks, slowed down the degradation rate of the SCM, controlled the gradual release of growth factors, and generated the constant supply of growth factors to cells [38-40]. In addition, cell viability is affected by calcium ions released from the SCM during degradation. The existence of fibrin from the PRP influenced calcium ion release, i.e., not too much and longer [41]. This study revealed that the degradation rate was not too much, even 96 h after being accelerated with an acidic solution. Under SEM observation, h-MSCs were found to attach, extend their processus, and proliferate after 48 h of incubation.

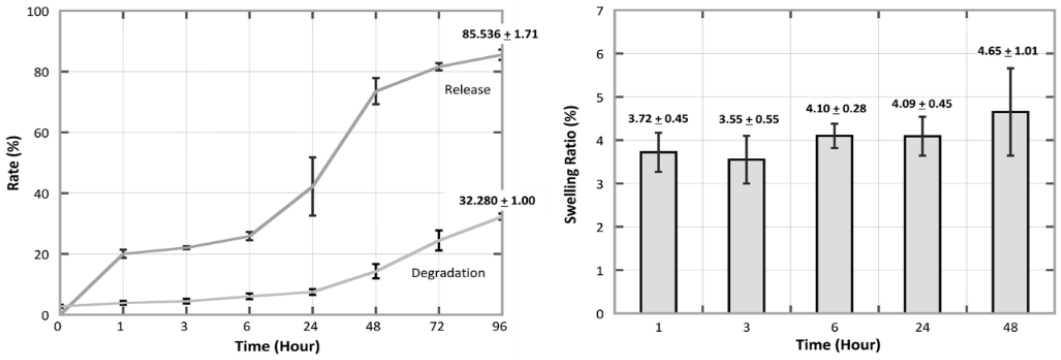

Figure 3 Degradation rate, release profile, and swelling ratio of the synthetic coral matrix (SCM) demonstrate adequate crosslinking procedure to maintain water sorption, avoid direct matrix degradation, and provide tunable release profile.

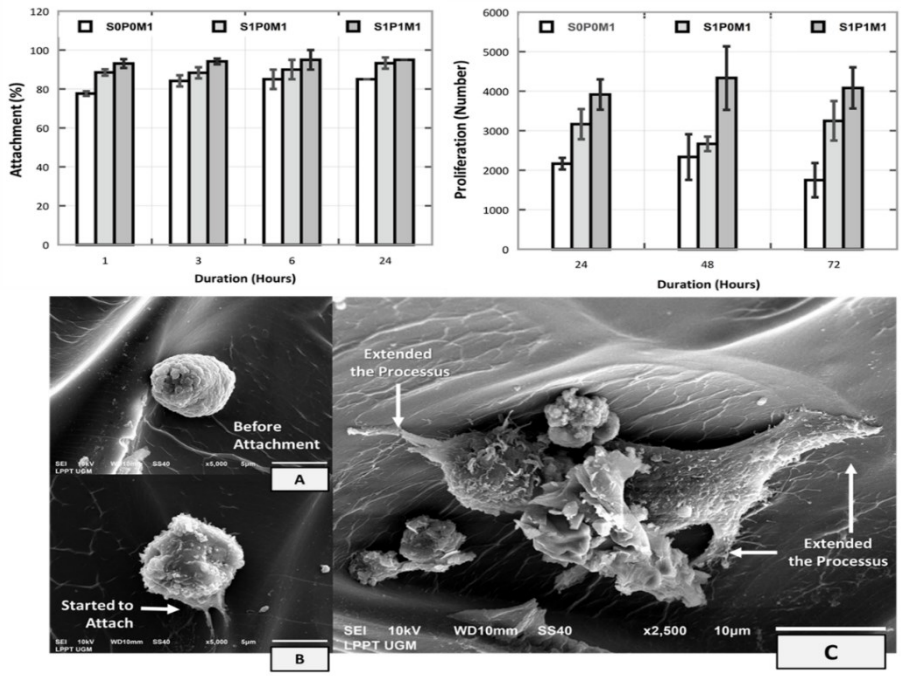

Figure 4 Percentage of h-MSC attachment and the number of proliferated cells in the culture without any scaffold (S0P0M1), culture with scaffold without PRP (S1P0M1), and culture with PRP (S1P1M1). Significant differences in the attachment and proliferation were found among samples, except in groups after 6 h of incubation ($p < 0.741$) for cell attachment and 48 h of incubation ($p < 0.138$) for cell proliferation. However, significant differences were found in all groups, except 48 h after incubation. A) Micrograph of the h-MSC before attachment and B) when h-MSCs started to attach (5000× magnification) after 48 h of incubation. h-MSCs were found to extend their processus 48 h after incubation (2500× magnification).

Regarding h-MSC differentiation in this study, runx2, osterix, and osteocalcin genes were chosen as biomarkers for osteoblast differentiation. Runx2 is expressed in the early stage of differentiation, coexisting with Type-1 collagen, LMP-1, Dlx5, alkaline phosphatase (ALP), osteopontin (OSP), osterix, FGF-receptor 3, TGF-β2, PTHrP, Dickkp2, and FGF-18 in the proliferative stage [42,43]. Runx2 is the most upstream transcription factor vital for osteoblast differentiation, regulates the expression of Sp7 protein for osteoblast differentiation and other bone matrix genes, and is essential for chondrocyte maturation [44]. Meanwhile, osterix is also one of the markers in the proliferative stage, which activates differentiation toward cell maturation. Osterix expression indicated that the cells did not differentiate into chondrocytes [45]. Furthermore, to detect the final differentiation process, osteocalcin is involved in the regulation of mineral deposition and acts as a bone matrix signal that promotes osteoblast differentiation and activation. Osteocalcin is expressed by osteoblasts alone as a marker of mature osteoblasts [46,47].

In this study, the highest runx2 expression on day 7 was found in S1P0M1-OM but not in S1P1M1-OM. This may be due to the faster expression of runx2 by the induction of SCM with PRP. Runx2 usually appears on day 8 of incubation; however, in the induced state, it could be expressed earlier. After the expression of runx2 reaches a peak, the expression will decrease [37,48]. In this study, runx2, the gene involved in the early differentiation stage, was expressed earlier in the presence of signaling molecules from the PRP, which regulated h-MSC differentiation. A corresponding phenomenon was also found in the expression of osterix on day 14. Furthermore, for osteocalcin expression on day 21, S1P1M1-OM had the highest expression level, whereas S1P1M1-SM had the lowest, which may be due to the lower capacity of SM to induce mineralization compared with OM which provided an osteogenic microenvironment to h-MSCs (**Figure 5**).

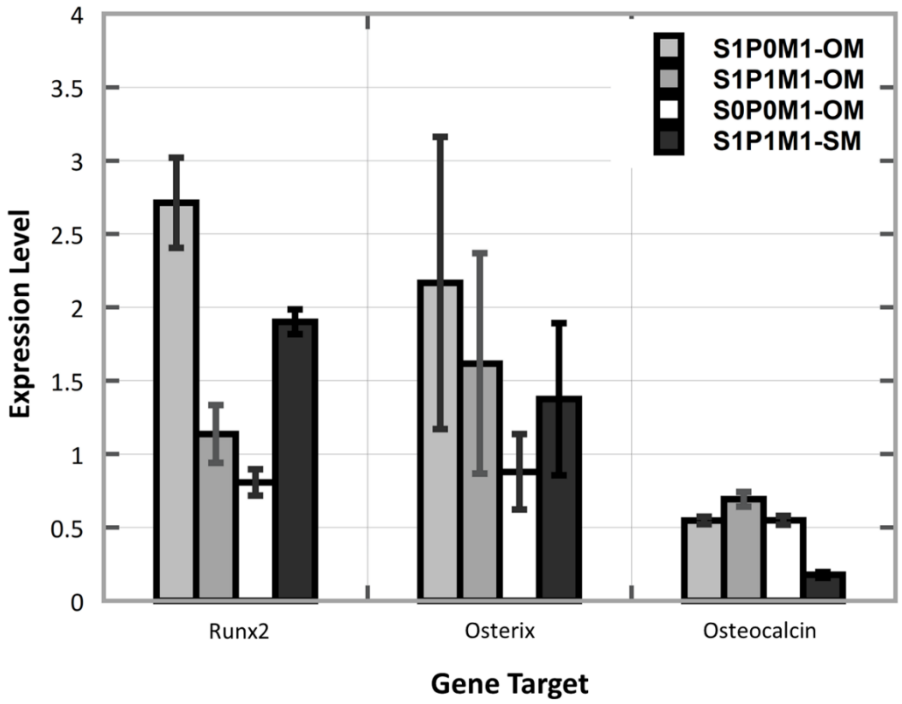

Figure 5 Expression level of Runx2, Osterix and Osteocalcin.

Ectopic bone formation

Bone formation in a nonosseous environment has been used as an indicator of ossification by osteoblasts. In this study, SCMs (S) were implanted in rat dorsum with (0) or without (1) growth factor cocktail from the PRP (P) and preincubated with (1) or without (0) h-MSCs. Histological staining with Mallory's trichrome of the subcutaneous tissues 3 weeks after implantation showed bone islands within the surviving SCMs in S1P1M1 and S1P0M1, indicating bone formation and collagen fiber production by osteoblast (**Figure 6**).

To confirm the formation of ectopic bone, IHC staining with osteocalcin was performed. The reactivity level to IHC staining was observed and scored by 2 independent observers, who were using a

Kappa value of 0.104. The results of IHC with osteocalcin corroborated the results of Mallory trichrome staining. The results of the IRS analysis are listed in **Table 2**. The S1P1M1 had the highest IRS, expressed by strongly positive immunoreactivity in weeks 3 and 4 after implantation, as also demonstrated in **Figure 7**. In S1P0M1 (group with SCM and MSCs but without growth factors from the PRP), moderate reactivity was detected since week 3 of the implantation. No significant relationships were found between reactivity with implantation duration and types of implanted matrices (S1P0M0, S1P0M1, S1P1M0, and S1P1M1) in weeks 1, 2, and 3 with the significance values of 0.484, 0.484, and 0.241, respectively. However, 4 weeks after implantation, the relationship was found significant ($p = 0.003$).

In vivo implantation of the SCM with or without PRP in a nonosseous tissue of rat dorsum exhibited different phenomena. *In vivo* cytoskeletogenesis is influenced by three signaling factors, i.e., pro-inflammatory cytokines (early phase), growth factors and differentiation (middle phase), and then metalloproteinases (MMP) and angiogenesis factors (late phase). After implantation injury, the tissue will react within 24 h. Inflammatory cells and local MSCs will secrete interleukin (IL)-1, IL-6, and tumor necrosis factor-α, which stimulate other inflammatory cells, ECM synthesis, MSC arrest, chondrocyte apoptosis, and osteoclast activity [49,50]. From the *in vivo* observation, the SCMs in the S1P0M0 and S1P1M0 had not fully degraded until week 2. Starting from week 3, the SCMs degraded, and no osteogenic differentiation was found. Upon S1P0M0 implantation, the inflammatory cell response failed to induce local SCs to differentiate into osteoblasts [51]. In S1P1M0, the same phenomenon occurred as in S1P0M0, even with PRP incorporation. This might occur because growth factors released through the SCM have failed to induce local cells to achieve osteogenic differentiation. A body response even showed phagocytosis of the SCM over time [52]. A different phenomenon may happen if the SCM is implanted in a bone area, because the bone environment (osseos) contains osteoprogenitors, preosteoblasts, and osteoblasts, which are not present in a nonosseous environment.

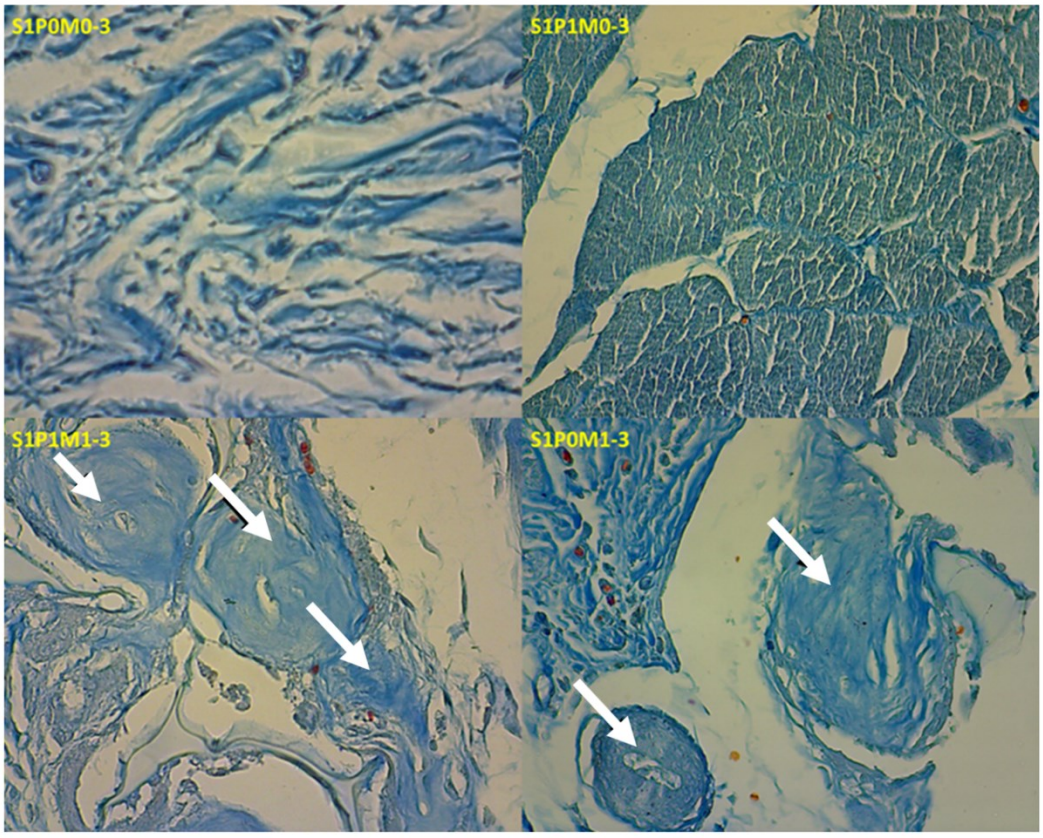

Figure 6 Mallory trichrome staining of rat dorsum 3 weeks after subcutaneous implantation (400× magnification). Arrows represent bone formation in the remaining synthetic coral matrices and the production of collagen fibers by osteoblasts.

In the middle phase, TGF-β and BMP act to stimulate cell growth and differentiation of SCs into osteoblasts. In the final phase, ECM degradation by MMP, and angiogenesis with vascular invasion begin.

MMPs 13 and 9 work together to degrade collagen and aggrecan to provide opportunities for vascular invasion. Vascular invasion for this angiogenesis is stimulated by VEGF secreted by chondrocytes during chondrocyte hypertrophy [53,54].

This study revealed differences between *in vitro* and *in vivo* conditions. The rate of SCM degradation is one of several differences, in which *in vivo* degradation takes longer than *in vitro*. Based on previous observations, implanted scaffolds could still support defective structures up to 6 and 8 weeks after implantation [52,55,56]. This allows cells to grow, develop, and deposit bone matrix. During *in vivo* implantation, local cells actively participate in the healing and formation of new bones. Local cells express and secrete growth factors and cytokines involved in bone formation [57]. For this, osteocalcin can act as a marker indicating osteoblast maturation, bone matrix deposition, and mineralization. In other words, osteocalcin can be a marker for bone formation [49].

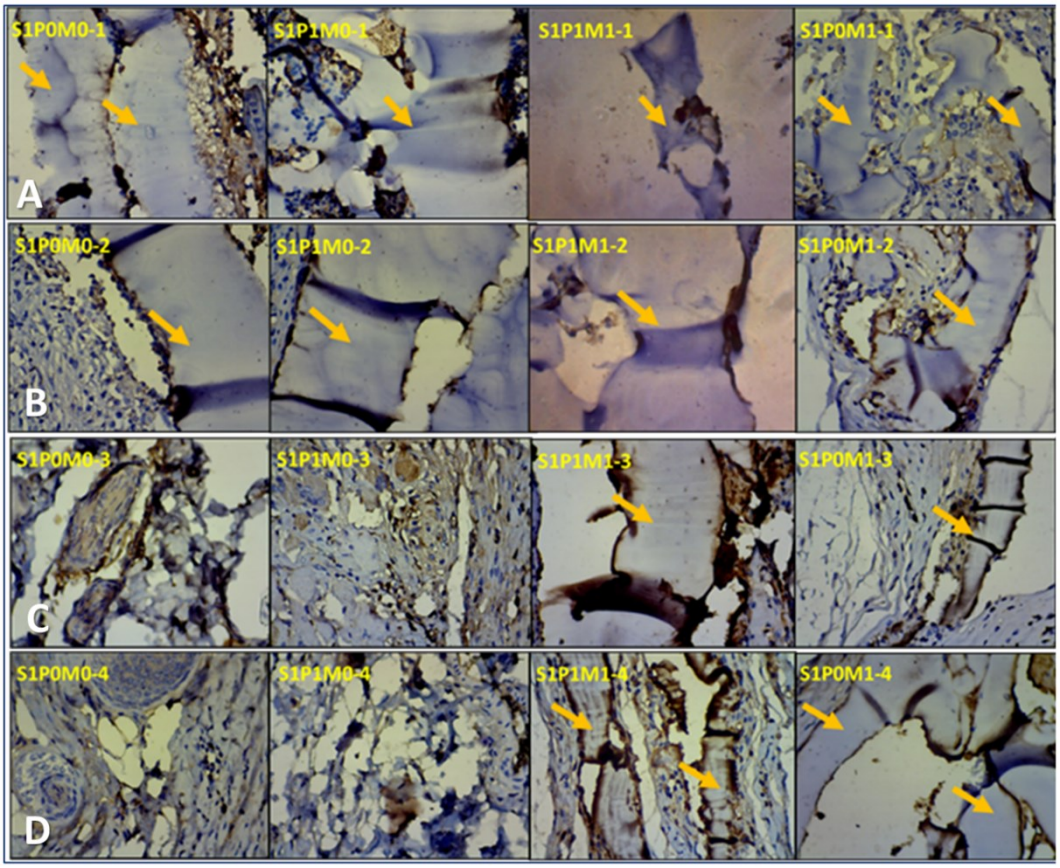

Figure 7 Immunohistochemistry staining for osteocalcin in the subcutaneous tissue on rat dorsum in A) week 1, B) week 2, C) week 3, and D) week 4 after implantation. The arrows show the remaining synthetic coral matrix. A positive response to osteocalcin is indicated by the appearance of a brown color. Histological analysis shows that the brownish color at the edge of the synthetic coral matrices started to spread into the matrices, indicating the presence of osteoblast and bone matrix production. Without MSCs, synthetic coral matrices started to degrade in week 3 of implantation. In the group with MSCs, synthetic matrices remained up to week 4 of implantation.

IHC using osteocalcin will express a brown color in the implanted SCM area. Bone matrix secretion and mineralization are indicated by the appearance of osteocalcin. S1P1M1 and S1P0M1 expressed a clear brown color at week 3, indicating the presence of mature osteoblasts. S1P1M1 preparations had a higher brown color intensity, which spread over the SCM area, indicating the spread of the bone matrix secreted by osteoblasts. In S1P0M1, ectopic bone formation occurred on week 3, even without PRP. In the *in vivo* environment, the implantation site still received growth factors such as TGF-β produced by proinflammatory cells and local cells, which can induce MSCs that have been attached to the scaffold to differentiate into osteoblasts. This was different from the *in vitro* conditions. In the *in vivo* conditions

without PRP, a steady supply of growth factors needed by MSCs for osteogenic differentiation can be obtained from inflammatory cells that generate growth factors [57,58].

Furthermore, S1P1M1 had a higher staining intensity than S1P0M1 because, in addition to obtaining growth factors from the implantation environment (inflammatory cells and local surrounding cells), S1P1M1 also obtained growth factors from PRP incorporated into the SCM, which are released along with the degradation of the SCM. In S1P0M1 and S1P1M1, the SCM was still on site until week 4. This is in line with the results of several previous studies, such as in [58,59], implanted various scaffold materials into the intramuscular area to evaluate ectopic bone formation until week 12 and distinguished them between scaffolds alone and cell-seeded scaffolds. This study validated the phenomena found in previous studies related to cell-seeded scaffolds [58,59], to the point that SCM degradation slowed down and allowed bone formation [51,58,59]. By contrast, the group without MSC, namely, S1P0M0, and S1P1M0, demonstrated rapid SCM degradation in week 3. The IHC results (**Figure 7**) are also in line with the results of histological staining with Mallory's trichrome (**Figure 6**) by the appearance of ectopic bone in the subcutaneous tissue in rat dorsum in S1P0M1 and S1P1M1 3 weeks after implantation. The incorporation of growth factor cocktails from the PRP into the SCM as a scaffold did not alter the results *in vivo*.

Table 2 Results of immunoreactivity score (IRS) of the IHC-stained subcutaneous tissues.

Duration of subcutaneous implantation (week)	Specimen number	Immunoreactivity Score (IRS)			
		S1P0M0	**S1P0M1**	**S1P1M0**	**S1P1M1**
1	1	Negative	Negative	Negative	Negative
	2	Negative	Negative	Mild	Negative
	3	Negative	Negative	Negative	Mild
2	1	Negative	Negative	Negative	Negative
	2	Negative	Negative	Negative	Negative
	3	Negative	Mild	Negative	Mild
3	1	Negative	Moderate	Negative	Moderate
	2	Mild	Negative	Mild	Moderate
	3	Negative	Negative	Negative	Strongly positive
4	1	Negative	Moderate	Negative	Strongly positive
	2	Negative	Moderate	Negative	Strongly positive
	3	Negative	Moderate	Negative	Moderate

Conclusions

In this study, SCM with high biocompatibility, good osteoconductivity, and resorbability, which can provide a bone growth factor delivery system, has been developed to resolve problems in using native corals for bone tissue engineering. The SCM provided an ideal microenvironment for h-MSCs to enhance bone regeneration process, indicated by faster, and high expression levels of runx2, osterix, and osteocalcin. The high capability of SCM with or without growth factor from the PRP to enhance bone formation has been proven from the ectopic bone formed in the nonosseous environment represented by subcutaneous rat dorsal tissue. This study also verified results of previous studies that implantation of scaffolds without cell seeding resulted in a lower rate of bone formation due to the faster degradation of the scaffold. Further studies and valorization phases are needed for the application of the results for bone tissue engineering in clinics.

Acknowledgements

Authors thank to Universitas Gadjah Mada (UGM), Indonesia for the support in post-doctoral program of Erlina Sih Mahanani, DDS., PhD. under contract number 13602/UN1.P.II/Dit-Lit/PT.01.04/2022.

References

[1] Y Tabata. Biomaterial technology for tissue engineering applications. *J. R. Soc. Interface* 2009; **6**, S311-S324.

[2] BP Chan and KW Leong. Scaffolding in tissue engineering: General approaches and tissue-specific considerations. *Eur. Spine J.* 2008; **17**, 467-79.

[3] SK Nandi, B Kundu, J Mukherjee, A Mahato, S Datta and VK Balla. Converted marine coral hydroxyapatite implants with growth factors: *In vivo* bone regeneration. *Mater. Sci. Eng. C* 2015; **49**, 816-23.

[4] D Srivastava and ND Witt. *In vivo* cellular reprogramming: The next generation. *Cell* 2016; **166**, 1386-96.

[5] CM Andreasen, JM Delaisse, BCVD Eerden, JPV Leeuwen, M Ding and TL Andersen. Understanding age-induced cortical porosity in women: The accumulation and coalescence of eroded cavities upon existing intracortical canals is the main contributor. *J. Bone Miner. Res.* 2018; **33**, 606-20.

[6] AI Birkhold, H Razi, R Weinkamer, GN Duda, S Checa and BM Willie. Monitoring *in vivo* (re) modeling: A computational approach using 4D micro-CT data to quantify bone surface movements. *Bone* 2015; **75**, 210-21.

[7] P Chocholata, V Kulda and Babuska. Fabrication of scaffolds for bone-tissue regeneration. *Materials* 2019; **12**, 568.

[8] H Pereira, IF Cengiz, FR Maia, F Bartolomeu, JM Oliveira, RL Reis and FS Silva. Physicochemical properties and cytocompatibility assessment of non-degradable scaffolds for bone tissue engineering applications. *J. Mech. Behav. Biomed. Mater*. 2020; **112**, 103997.

[9] ID Ana*. Bone substituting materials in dental implantology*. *In*: AS Budihardja and T Mücke (Eds.). Bone management in dental implantology. Springer, Cham, Switzerland, 2019, p. 121-4.

[10] L Guo, Z Liang, L Yang, W Du, T Yu, H Tang, C Li and H Qiu. The role of natural polymers in bone tissue engineering. *J. Contr. Release* 2021; **338**, 571-82.

[11] N Aslankoohi, D Mondal, AS Rizkalla and K Mequanint. Bone repair and regenerative biomaterials: Towards recapitulating the microenvironment. *Polymers* 2019; **11**, 1437.

[12] R Shi, Y Huang, C Ma, C Wu and W Tian. Current advances for bone regeneration based on tissue engineering strategies. *Front Med.* 2019; **13**, 160-88.

[13] P Wang, L Zhao, J Liu, MD Weir, X Zhou and HH Xu. Bone tissue engineering via nanostructured calcium phosphate biomaterials and stem cells. *Bone Res.* 2014; **30**, 14017.

[14] Y Qian, Q Han, W Chen, J Song, X Zhao, Y Ouyang, W Yuan and C Fan. Platelet-rich plasma derived growth factors contribute to stem cell differentiation in musculoskeletal regeneration. *Front Chem*. 2017; **5**, 89.

[15] ID Ana. *Hybrid biomaterials in drug delivery and biomedical applications. In*: S Jana and S Jana (Eds.). Functional Biomaterials. Springer Nature, Singapore, 2022, p. 409-34.

[16] R Hou, F Chen, Y Yang, X Cheng, Z Gao, HO Yang, W Wu and T Mao. Comparative study between coral-mesenchymal stem cells-rhBMP-2 composite and auto-bone-graft in rabbit critical-sized cranial defect model. *J. Biomed. Mater. Res. A* 2007; **80**, 85-93.

[17] AS Neto and JMF Ferreira. Synthetic and marine-derived porous scaffolds for bone tissue engineering. *Materials* 2018; **11**, 1702.

[18] KA Al-Salihi. *In vitro* evaluation of Malaysian natural coral porites bone graft substitutes (CORAGRAF) for bone tissue engineering: A preliminary study. *Braz. J. Oral Sci*. 2009; **8**, 210-6.

[19] ES Mahanani, I Bachtiar and ID Ana. Human mesenchymal stem cells behaviour on synthetic coral scaffold. *Key Eng. Mater*. 2016; **696**, 205-11.

[20] V Viateau, M Manassero, L Sensébé, A Langonné, D Marchat, D Logeart-Avramoglou, H Petite and M Bensidhoum. Comparative study of the osteogenic ability of four different ceramic constructs in an ectopic large animal model. *J. Tissue Eng. Regen. Med*. 2016; **10**, E177-E187.

[21] A Patriati, R Ardhani, HD Pranowo, EGR Putra and ID Ana. The effect of freeze-thaw treatment to the properties of gelatin-carbonated hydroxyapatite membrane for nerve regeneration scaffold. *Key Eng. Mater*. 2016; **696**, 129-44.

[22] AA Alhasyimi, PP Pudyani, W Asmara and ID Ana. Enhancement of post-orthodontic tooth stability by carbonated hydroxyapatite-incorporated advanced platelet-rich fibrin in rabbits. *Orthod. Craniofac. Res*. 2018; **21**, 112-8.

[23] M Matsui and Y Tabata. Enhanced angiogenesis by multiple release of platelet-rich plasma contents and basic fibroblast growth factor from gelatin hydrogels. *Acta Biomaterialia* 2012; **8**, 1792-801.

[24] R Ardhani, S Setyaningsih, OA Hafiyyah and ID Ana. Preparation of carbonated apatite membrane as metronidazole delivery system for periodontal application. *Key Eng. Mater.* 2016; **696**, 250-8.
[25] N Fedchenko and J Reifenrath. Different approaches for interpretation and reporting of immunohistochemistry analysis results in the bone tissue - a review. *Diagn. Pathol*. 2014; **9**, 221.
[26] F Dickens. The citric acid content of animal tissues, with reference to its occurrence in bone and tumour. *Biochem. J*. 1941; **35**, 1011-23.
[27] SC Leeuwenburgh, ID Ana and JA Jansen. Sodium citrate as an effective dispersant for the synthesis of inorganic-organic composites with a nanodispersed mineral phase. *Acta Biomaterialia* 2010; **6**, 836-44.
[28] S Elangovan, SR D'Mello, L Hong, RD Ross, C Allamargot, DV Dawson, CM Stanford, GK Johnson, DR Sumner and AK Salem. The enhancement of bone regeneration by gene activated matrix encoding for platelet derived growth factor. *Biomaterials* 2014; **35**, 737-47.
[29] R Sakata and AH Reddi. Platelet-rich plasma modulates actions on articular cartilage lubrication and regeneration. *Tissue Eng. B Rev.* 2016; **22**, 408-19.
[30] JP Konsek, J Knaus, J Avaro, EV Sturm and H Cölfen. Cross-linking of apatite-gelatin nanocomposites as the basis for dentine replacement materials. *ACS Biomater. Sci. Eng*. 2023; **9**, 1815-22.
[31] MG Haugh, CM Murphy, RC McKiernan, C Altenbuchner and FJ O'Brien. Crosslinking and mechanical properties significantly influence cell attachment, proliferation, and migration within collagen glycosaminoglycan scaffolds. *Tissue Eng. A* 2011; **17**, 1201-8.
[32] GB Schneider, A English, M Abraham, R Zaharias, C Stanford and J Keller. The effect of hydrogel charge density on cell attachment. *Biomaterials* 2004; **25**, 3023-8.
[33] CN Grover, JH Gwynne, N Pugh, S Hamaia, RW Farndale, SM Best and RE Cameron. Crosslinking and composition influence the surface properties, mechanical stiffness and cell reactivity of collagen-based films. *Acta Biomaterialia* 2012; **8**, 3080-90.
[34] P Kaur. Platelet-rich plasma: A novel bioengineering concept. *Trends Biomater. Artif. Organs* 2011; **25**, 86-90.
[35] RJ Miron, M Fujioka-Kobayashi, M Bishara, Y Zhang, M Hernandez and J Choukroun. Platelet-rich fibrin and soft tissue wound healing: A systematic review. *Tissue Eng. B Rev*. 2017; **23**, 83-99.
[36] E Anitua, M Zalduendo, M Troya, R Tierno and MH Alkhraisat. The inclusion of leukocytes into platelet rich plasma reduces scaffold stability and hinders extracellular matrix remodeling. *Ann. Anat*. 2022; **240**, 151853.
[37] M Igarashi, N Kamiya, M Hasegawa, T Kasuya, T Takahashi and M Takagi. Inductive effects of dexamethasone on the gene expression of Cbfa1, Osterix and bone matrix proteins during differentiation of cultured primary rat osteoblasts. *J. Mol. Histol*. 2004; **35**, 3-10.
[38] E Carletti, A Motta and C Migliaresi. Scaffolds for tissue engineering and 3D cell culture. *Meth. Mol. Biol*. 2011; **695**, 17-39.
[39] Z Söderlund, A Ibáñez-Fonseca, S Hajizadeh, JC Rodríguez-Cabello, J Liu, L Ye, E Tykesson, L Elowsson and G Westergren-Thorsson. Controlled release of growth factors using synthetic glycosaminoglycans in a modular macroporous scaffold for tissue regeneration. *Comm. Biol*. 2022; **5**, 1349.
[40] MM Ammar, GH Waly, SH Saniour and TA Moussa. Growth factor release and enhanced encapsulated periodontal stem cells viability by freeze-dried platelet concentrate loaded thermo-sensitive hydrogel for periodontal regeneration. *Saudi Dent. J*. 2018; **30**, 355-64.
[41] M Gruening, S Neuber, P Nestler, J Lehnfeld, M Dubs, K Fricke, M Schnabelrauch, CA Helm, R Müller, S Staehlke and JB Nebe. Enhancement of intracellular calcium ion mobilization by moderately but not highly positive material surface charges. *Front. Bioeng. Biotechnol*. 2020; **8**, 1016.
[42] M Cámara-Torres, R Sinha, A Sanchez, P Habibovic, A Patelli, C Mota and L Moroni. Effect of high content nanohydroxyapatite composite scaffolds prepared via melt extrusion additive manufacturing on the osteogenic differentiation of human mesenchymal stromal cells. *Biomater. Adv*. 2022; **137**, 212833.
[43] P Kasten, J Vogel, I Beyen, S Weiss, P Niemeyer, A Leo and R Lüginbuhl. Effect of platelet-rich plasma on the *in vitro* proliferation and osteogenic differentiation of human mesenchymal stem cells on distinct calcium phosphate scaffolds: The specific surface area makes a difference. *J. Biomater. Appl*. 2008; **23**, 169-88.
[44] T Komori. Roles of Runx2 in skeletal development. *Adv. Exp. Med. Biol*. 2017; **962**, 83-93.

[45] X Zhou, Z Zhang, JQ Feng, VM Dusevich, K Sinha, H Zhang, BG Darnay and BD Crombrugghe. Multiple functions of Osterix are required for bone growth and homeostasis in postnatal mice. *Proc. Natl. Acad. Sci. Unit. States Am.* 2010; **107**, 12919-24.
[46] A Neve, A Corrado and EP Cantatore. Osteoblast physiology in normal and pathological conditions. *Cell Tissue Res*. 2011; **343**, 289-302.
[47] SY Lu, CY Wang, Y Jin, Q Meng, Q Liu, ZH Liu, KX Liu, HJ Sun and MZ Liu. The osteogenesis-promoting effects of alpha-lipoic acid against glucocorticoid-induced osteoporosis through the NOX4, NF-kappaB, JNK and PI3K/AKT pathways. *Sci. Rep*. 2017; **7**, 3331.
[48] KM Sinha and X Zhou. Genetic and molecular control of osterix in skeletal formation. *J. Cell. Biochem*. 2013; **114**, 975-84.
[49] U Kini and BN Nandeesh. *Enhanced reader*. *In*: I Fogelman, G Gnanasegaran and H Wall (Eds.). Radionuclide and hybrid bone imaging. Springer, Berlin, Germany, 2012, p. 29-57.
[50] DS Amarasekara, S Kim and J Rho. Regulation of osteoblast differentiation by cytokine networks. *Int. J. Mol. Sci*. 2021; **22**, 2851.
[51] YC Chai, L Geris, J Bolander, G Pyka, S Van Bael, FP Luyten, J Schrooten. *In vivo* ectopic bone formation by devitalized mineralized stem cell carriers produced under mineralizing culture condition. *Biores Open Access* 2014; **3**, 265-77.
[52] AR Costa-Pinto, AM Martins, M Castelhano-Carlos, VM Correlo, PC Sol, A Longatto-Filho, M Battacharya, RL Reis and NM Neves. *In vitro* degradation and *in vivo* biocompatibility assessment of chitosan-poly(butylene succinate) fiber mesh scaffolds. *J. Bioact. Compat. Polym*. 2014; **29**, 137-51.
[53] S Bartaula-Brevik, TO Pedersen, A Finne-Wistrand, AI Bolstad and K Mustafa. Angiogenic and immunomodulatory properties of endothelial and mesenchymal stem cells. *Tissue Eng. A* 2016; **22**, 244-52.
[54] Y Man, P Wang, Y Guo, L Xiang, Y Yang, Y Qu, P Gong and L Deng. Angiogenic and osteogenic potential of platelet-rich plasma and adipose-derived stem cell laden alginate microspheres. *Biomaterials* 2012; **33**, 8802-11.
[55] CE Raposo-Amaral, DF Bueno, AB Almeida, V Jorgetti, CC Costa, CH Gouveia, LC Vulcano, RD Fanganiello, MR Passos-Bueno and N Alonso. Is bone transplantation the gold standard for repair of alveolar bone defects? *J. Tissue Eng*. 2014; **5**, 1-11.
[56] AH Dewi, ID Ana, J Wolke and J Jansen. Behavior of POP-calcium carbonate hydrogel as bone substitute with controlled release capability: A study in rat. *J. Biomed. Mater. Res. A* 2015; **103**, 3273-83.
[57] S Sundelacruz and DL Kaplan. Stem cell- and scaffold-based tissue engineering approaches to osteochondral regenerative medicine. *Semin. Cell Dev. Biol*. 2009; **20**, 646-55.
[58] J Jin, J Wang, J Huang, F Huang, J Fu, X Yang and Z Miao. Transplantation of human placenta-derived mesenchymal stem cells in a silk fibroin/hydroxyapatite scaffold improves bone repair in rabbits. *J. Biosci. Bioeng*. 2014; **118**, 593-8.
[59] JO Eniwumide, H Yuan, SH Cartmell, GJ Meijer and JDD Bruijn. Ectopic bone formation in bone marrow stem cell seeded calcium phosphate scaffolds as compared to autograft and (cell seeded) allograft. *Eur. Cell. Mater*. 2007; **14**, 30-8.